Multidimensional generalized-ensemble algorithms for complex systems

Ayori Mitsutake[1,a)] and Yuko Okamoto[2,b)]
[1]*Department of Physics, Keio University, Yokohama, Kanagawa 223-8522, Japan*
[2]*Department of Physics, Nagoya University, Nagoya, Aichi 464-8602, Japan*

(Received 4 March 2009; accepted 13 April 2009; published online 4 June 2009)

We give general formulations of the multidimensional multicanonical algorithm, simulated tempering, and replica-exchange method. We generalize the original potential energy function E_0 by adding any physical quantity V of interest as a new energy term. These multidimensional generalized-ensemble algorithms then perform a random walk not only in E_0 space but also in V space. Among the three algorithms, the replica-exchange method is the easiest to perform because the weight factor is just a product of regular Boltzmann-like factors, while the weight factors for the multicanonical algorithm and simulated tempering are not *a priori* known. We give a simple procedure for obtaining the weight factors for these two latter algorithms, which uses a short replica-exchange simulation and the multiple-histogram reweighting techniques. As an example of applications of these algorithms, we have performed a two-dimensional replica-exchange simulation and a two-dimensional simulated-tempering simulation using an α-helical peptide system. From these simulations, we study the helix-coil transitions of the peptide in gas phase and in aqueous solution. © *2009 American Institute of Physics*. [DOI: 10.1063/1.3127783]

I. INTRODUCTION

Canonical fixed-temperature simulations of complex systems such as biopolymers are greatly hampered by the multiple-minima problem. Because simulations at low temperatures tend to get trapped in a few of a huge number of local-minimum-energy states which are separated by high-energy barriers, it is very difficult to obtain accurate canonical distributions at low temperatures by conventional Monte Carlo (MC) and molecular dynamics (MD) simulations. One way to overcome this multiple-minima problem is to perform a simulation in a *generalized ensemble* where each state is weighted by an artificial, non-Boltzmann probability weight factor so that a random walk in potential energy space may be realized (for reviews see, e.g., Refs. 1–5). The random walk allows the simulation to overcome any energy barrier and to sample a much wider configurational space than by conventional methods. Monitoring the energy in a single simulation run, one can obtain not only the global-minimum-energy state but also canonical-ensemble averages as functions of temperature by the single-histogram[6] and/or multiple-histogram[7,8] reweighting techniques [an extension of the multiple-histogram method is also referred to as the *weighted histogram analysis method*[8] (WHAM)].

Three of well-known generalized-ensemble algorithms are *multicanonical algorithm* (MUCA),[9,10] *simulated tempering* (ST),[11,12] and *replica-exchange method* (REM).[13,14] MUCA is also referred to as *adaptive umbrella sampling*[15] *of the potential energy*.[16] ST is also referred to as the *method of expanded ensemble*[11] and for a review, see, e.g., Ref. 17. The REM is also referred to as *multiple Markov chain method*[18] and *parallel tempering*.[17] In MUCA, ST, and REM, random walks in potential energy (MUCA) and temperature (ST and REM) are realized.

MUCA was introduced to the chemical physics field in Ref. 19, ST was in Refs. 11 and 20–22, and REM was in Refs. 23–27. The MD version of MUCA was developed in Refs. 28 and 29. The details of MD algorithm have also been worked out for REM in Ref. 24 [it is referred to as Replica-Exchange Molecular Dynamics (REMD)]. This led to a wide application of REM in the protein folding and related problems (see, e.g., Refs. 30–41).

MUCA has been extended so that random walks in other parameters instead of energy may be obtained.[42–48] Moreover, two-dimensional (or two-component) extensions of MUCA can be found in Refs. 44, 45, and 49–51. One is also naturally led to a multidimensional (or multivariable) extension of REM, which we refer to as *multidimensional replica-exchange method* (MREM),[52] where not only temperature but also other parameters of the system is exchanged in the replica-exchange process. An example of two-dimensional REM is temperature-pressure replica exchange.[3,53,54] A special realization of MREM is *replica-exchange umbrella sampling*[52,55] and it is particularly useful in free energy calculations (see also Ref. 56 for a similar idea). MREM is also referred to as *generalized parallel sampling*,[57] *Hamiltonian REM*,[58] *REM using the generalized effective potential*,[59] and *model hopping*.[60] The MREM formulation[52] led to many extensions of REM where parameters in the potential energy other than temperature (or special ensembles of the systems) are exchanged (see, for instance, Refs. 2, 3, and 61–69). Finally, ST can be extended to a multidimensional version as described below in detail.

In this article, we present general formulations of the multidimensional generalized-ensemble algorithms such as multidimensional MUCA, multidimensional ST, and MREM. We generalize the original potential energy function E_0 by

[a)]Electronic mail: ayori@mail.rk.phys.keio.ac.jp.
[b)]Electronic mail: okamoto@phys.nagoya-u.ac.jp.

adding any physical quantities of interest V_ℓ as a new energy term with coupling constants $\lambda^{(\ell)}, (\ell=1,\ldots,L)$. Preliminary results have been reported elsewhere.[70]

While the REM simulation can be easily performed because no weight factor determination is necessary, the required number of replicas can become quite large and computationally demanding. From previous works,[5,62,63,65] it was also shown that the random walks in the MUCA and ST simulations are more enhanced than that in the REM simulation. We thus prefer to use MUCA or ST, where only a single replica is simulated, instead of REM. However, the weight factors of MUCA and ST simulations are not known *a priori* and we need to estimate them. It is very difficult to obtain optimal weight factors for MUCA and ST. In the previous works,[61–63,65,71] we proposed powerful methods to determine these weight factors. Namely, we first perform a short REM simulation and use the multiple-histogram reweighting techniques to determine the weight factors of MUCA and ST. In the present article, we describe the method to determine the weight factors for the multidimensional MUCA and ST by employing the MREM and the generalized multiple-histogram reweighting techniques.

As a test of the effectiveness of the methods, we have performed the two-dimensional REM simulation and the two-dimensional ST simulation of an α-helical peptide system with a solvent model. The weight factor for the two-dimensional ST simulation was obtained by the two-dimensional REM simulation.

The present article is organized as follows. In Sec. II, we describe the methods. In particular, in Sec. II A, we present our generalized energy function. In Secs. II B, II C, and II D, the multidimensional MUCA, the multidimensional ST, and the multidimensional REM are described, respectively. In Sec. II E, we explain the method to determine the weight factors for the multidimensional MUCA and the multidimensional ST by using the multidimensional REM and the multiple-histogram reweighting techniques. Here, we generalize the multiple-histogram reweighting techniques for the multidimensional version. In Sec. II F, we describe the methods to calculate averages of physical quantities from these simulations. In Sec. III, we give computational details of the two-dimensional REM simulation and two-dimensional ST simulation for a 17 residue α-helical peptide system with a model solvent. In Sec. IV, we present the results. Especially, in Secs. IV A, IV B, and IV C, we discuss the results of the two-dimensional REM simulation, the two-dimensional ST simulation, and detailed analysis of the solvent effects, respectively. In Sec. V, we conclude the article.

II. METHODS

A. Generalized energy function

Let us consider a generalized potential energy function $E_{\boldsymbol{\lambda}}(x)$ of a system in state x, which depends on L parameters $\boldsymbol{\lambda}=(\lambda^{(1)},\ldots,\lambda^{(L)})$. Although $E_{\boldsymbol{\lambda}}(x)$ can be any function of $\boldsymbol{\lambda}$, we consider the following specific generalized potential energy function:

$$E_{\boldsymbol{\lambda}}(x) = E_0(x) + \sum_{\ell=1}^{L} \lambda^{(\ell)} V_\ell(x). \tag{1}$$

Here, there are $L+1$ energy terms, $E_0(x)$, and $V_\ell(x)(\ell=1,\ldots,L)$, and $\lambda^{(\ell)}$ are the corresponding coupling constants for $V_\ell(x)$.

After integrating out the momentum degrees of freedom, the partition function of the system at fixed temperature T and parameters $\boldsymbol{\lambda}$ is given by

$$\begin{aligned} Z(T,\boldsymbol{\lambda}) &= \int dx \exp(-\beta E_{\boldsymbol{\lambda}}(x)) \\ &= \int dE_0 dV_1,\ldots,dV_L n(E_0,V_1,\ldots,V_L) \\ &\quad \times \exp(-\beta E_{\boldsymbol{\lambda}}), \end{aligned} \tag{2}$$

where $n(E_0,V_1,\cdots,V_L)$ is the multidimensional density of states:

$$\begin{aligned} n(E_0,V_1,\ldots,V_L) &= \int dx \delta(E_0(x)-E_0)\delta(V_1(x)-V_1) \\ &\quad \ldots \delta(V_L(x)-V_L), \end{aligned} \tag{3}$$

$\beta=1/k_BT$, and k_B is the Boltzmann constant. Here, the integration is replaced by a summation when x is discrete.

The expression in Eq. (1) is often used in simulations. For instance, in simulations of spin systems, $E_0(x)$ and $V_1(x)$ (here, $L=1$ and $x=\{S_1,S_2,\ldots\}$ stand for spins) can be respectively considered as the zero-field term and the magnetization term coupled with the external field $\lambda^{(1)}$. (For Ising model, $E_0=-J\Sigma_{\langle i,j\rangle}S_iS_j$, $V_1=-\Sigma_iS_i$, and $\lambda^{(1)}=h$, i.e., external magnetic field.) In umbrella sampling[72] in molecular simulations, $E_0(x)$ and $V_\ell(x)$ can be taken as the original potential energy and the (biasing) umbrella potential energy, respectively, with the coupling parameter $\lambda^{(\ell)}$ (here, $x=\{\boldsymbol{q}_1,\ldots,\boldsymbol{q}_N\}$ where $\boldsymbol{q}_i$ are the coordinate vectors of the ith particle and N is the total number of particles). For the molecular simulations in the isobaric-isothermal ensemble, $E_0(x)$ and $V_1(x)$ (here, $L=1$) correspond to the potential energy U and the volume $\mathcal{V}$ coupled with the pressure $\mathcal{P}$, respectively. (Namely, we have $x=\{\boldsymbol{q}_1,\cdots,\boldsymbol{q}_N,\mathcal{V}\}$, $E_0=U$, $V_1=\mathcal{V}$, and $\lambda^{(1)}=\mathcal{P}$, i.e., $E_{\boldsymbol{\lambda}}$ is the enthalpy without the kinetic energy contributions.) For simulations in the grand canonical ensemble with N particles, we have $x=\{\boldsymbol{q}_1,\ldots,\boldsymbol{q}_N,N\}$, and $E_0(x)$ and $V_1(x)$ (here, $L=1$) correspond to the potential energy U and the total number of particles N coupled with the chemical potential μ, respectively. (Namely, we have $E_0=U$, $V_1=N$, and $\lambda^{(1)}=-\mu$.) We remark that generalized-ensemble algorithms in various ensembles are also discussed in Refs. 73 and 74.

Moreover, going beyond the well-known ensembles discussed above, we can introduce any physical quantity of interest (or its function) as the additional potential energy term V_ℓ. For instance, V_ℓ can be an overlap with a reference configuration in spin glass systems, an end-to-end distance, a radius of gyration in molecular systems, etc. In such a case, we have to carefully choose the range of $\lambda^{(\ell)}$ values so that the new energy term $\lambda^{(\ell)}V_\ell$ will have roughly the same order

of magnitude as the original energy term E_0. We want to perform a simulation where a random walk not only in the E_0 space but also in the V_ℓ space is realized. As shown below, this can be done by performing a multidimensional MUCA, ST, or REM simulation.

B. Multidimensional multicanonical algorithm

The original MUCA can realize a one-dimensional random walk in potential energy space. The MUCA algorithms can be generalized to multidimensional ones. In this subsection, we describe the multidimensional MUCA simulation which realizes a random walk in the $(L+1)$-dimensional space of $E_0(x)$ and $V_\ell(x)(\ell=1,\ldots,L)$.

In the multidimensional MUCA ensemble, each state is weighted by the MUCA weight factor $W_{\mathrm{MU}}(E_0,V_1,\ldots,V_L)$ so that a uniform energy distribution of E_0, V_1,..., and V_L may be obtained:

$$P_{\mathrm{MU}}(E_0,V_1,\ldots,V_L) \propto n(E_0,V_1,\ldots,V_L) \times W_{\mathrm{MU}}(E_0,V_1,\ldots,V_L) \equiv \mathrm{const}, \tag{4}$$

where $n(E_0,V_1,\ldots,V_L)$ is the multidimensional density of states. From this equation, we obtain

$$W_{\mathrm{MU}}(E_0,V_1,\ldots,V_L) \equiv \exp(-\beta_a E_{\mathrm{MU}}(E_0,V_1,\ldots,V_L)) \propto \frac{1}{n(E_0,V_1,\ldots,V_L)}, \tag{5}$$

where we have introduced an arbitrary reference temperature, $T_a=1/k_B\beta_a$, and wrote the weight factor in the Boltzmann-like form. Here, the *multicanonical potential energy* is defined by

$$E_{\mathrm{MU}}(E_0,V_1,\ldots,V_L) \equiv k_B T_a \ln n(E_0,V_1,\ldots,V_L). \tag{6}$$

The multidimensional MUCA MC simulation can be performed with the following Metropolis transition probability[75] from state x with energy $E_{\boldsymbol{\lambda}}=E_0+\Sigma_{\ell=1}^{L}\lambda^{(\ell)}V_\ell$ to state x' with energy $E'_{\boldsymbol{\lambda}}=E'_0+\Sigma_{\ell=1}^{L}\lambda^{(\ell)}V'_\ell$:

$$w(x\to x') = \min\left(1,\frac{W_{\mathrm{MU}}(E'_0,V'_1,\ldots,V'_L)}{W_{\mathrm{MU}}(E_0,V_1,\ldots,V_L)}\right) = \min\left(1,\frac{n(E_0,V_1,\ldots,V_L)}{n(E'_0,V'_1,\ldots,V'_L)}\right). \tag{7}$$

A MD algorithm in the multidimensional MUCA ensemble also naturally follows from Eq. (5), in which a regular constant temperature MD simulation (with $T=T_a$) is performed by replacing the total potential energy $E_{\boldsymbol{\lambda}}$ by the multicanonical potential energy E_{MU} in Newton's equations for the kth particle $(k=1,\ldots,N)$ (see Refs. 28 and 29 for the one-dimensional version),

$$\dot{\boldsymbol{p}}_k = -\frac{\partial E_{\mathrm{MU}}(E_0,V_1,\ldots,V_L)}{\partial \boldsymbol{q}_k}. \tag{8}$$

C. Multidimensional simulated tempering

We now consider a multidimensional ST simulation which realizes a random walk both in temperature T and in parameters $\boldsymbol{\lambda}$. The entire parameter set $\boldsymbol{\Lambda}=(T,\boldsymbol{\lambda}) \equiv (T,\lambda^{(1)},\ldots,\lambda^{(L)})$ becomes dynamical variables and both the configuration and the parameter set are updated during the simulation with a weight factor

$$W_{\mathrm{ST}}(\boldsymbol{\Lambda}) \equiv \exp(-\beta E_{\boldsymbol{\lambda}} + f(\boldsymbol{\Lambda})), \tag{9}$$

where the function $f(\boldsymbol{\Lambda})=f(T,\boldsymbol{\lambda})$ is chosen so that the probability distribution of $\boldsymbol{\Lambda}$ is flat:

$$P_{\mathrm{ST}}(\boldsymbol{\Lambda}) \propto \int dE_0 dV_1,\ldots,dV_L n(E_0,V_1,\ldots,V_L) \times \exp(-\beta E_{\boldsymbol{\lambda}} + f(\boldsymbol{\Lambda})) \equiv \mathrm{const}. \tag{10}$$

This means that $f(\boldsymbol{\Lambda})$ is the dimensionless ("Helmholtz") free energy:

$$\exp(-f(\boldsymbol{\Lambda})) = \int dE_0 dV_1,\ldots,dV_L n(E_0,V_1,\ldots,V_L) \times \exp(-\beta E_{\boldsymbol{\lambda}}). \tag{11}$$

In the numerical work we discretize the parameter set $\boldsymbol{\Lambda}$ in $M(=M_0\times M_1\times\cdots\times M_L)$ different values: $\boldsymbol{\Lambda}_m \equiv (T_{m_0},\boldsymbol{\lambda}_m) \equiv (T_{m_0},\lambda^{(1)}_{m_1},\ldots,\lambda^{(L)}_{m_L})$, where $m_0=1,\ldots,M_0, m_\ell=1,\ldots,M_\ell(\ell=1,\ldots,L)$. Without loss of generality we can order the parameters so that $T_1<T_2<\cdots<T_{M_0}$ and $\lambda^{(\ell)}_1<\lambda^{(\ell)}_2<\cdots<\lambda^{(\ell)}_{M_\ell}$ (for each $\ell=1,\ldots,L$). The free energy $f(\boldsymbol{\Lambda}_m)$ is now written as $f_{m_0,m_1,\ldots,m_L}=f(T_{m_0},\lambda^{(1)}_{m_1},\ldots,\lambda^{(L)}_{m_L})$.

Once the initial configuration and the initial parameter set are chosen, the multidimensional ST is realized by alternately performing the following two steps:

(1) A "canonical" MC or MD simulation at the fixed parameter set $\boldsymbol{\Lambda}_m=(T_{m_0},\boldsymbol{\lambda}_m)=(T_{m_0},\lambda^{(1)}_{m_1},\ldots,\lambda^{(L)}_{m_L})$ is carried out for a certain steps with the weight factor $\exp(-\beta_{m_0}E_{\boldsymbol{\lambda}_m})$ [for fixed $\boldsymbol{\Lambda}_m$, $f(\boldsymbol{\Lambda}_m)$ in Eq. (9) does not contribute].

(2) We update the parameter set $\boldsymbol{\Lambda}_m$ to a new parameter set $\boldsymbol{\Lambda}_{m\pm1}$ in which one of the parameters in $\boldsymbol{\Lambda}_m$ is changed to a neighboring value with the configuration and the other parameters fixed. The transition probability of this parameter updating process is given by the following Metropolis criterion:

$$w(\boldsymbol{\Lambda}_m\to\boldsymbol{\Lambda}_{m\pm1}) = \min\left(1,\frac{W_{\mathrm{ST}}(\boldsymbol{\Lambda}_{m\pm1})}{W_{\mathrm{ST}}(\boldsymbol{\Lambda}_m)}\right) = \min(1,\exp(-\Delta)). \tag{12}$$

Here, there are two possibilities for $\boldsymbol{\Lambda}_{m\pm1}$, namely, T- and $\lambda^{(\ell)}$-updates. For T-update, we have $\boldsymbol{\Lambda}_{m\pm1}=(T_{m_0\pm1},\boldsymbol{\lambda}_m)$ with

$$\Delta = (\beta_{m_0\pm1}-\beta_{m_0})E_{\boldsymbol{\lambda}_m} - (f_{m_0\pm1,m_1,\ldots,m_L} - f_{m_0,m_1,\ldots,m_L}). \tag{13}$$

For $\lambda^{(\ell)}$-update (for one of $\ell=1,\ldots,L$), we have $\boldsymbol{\Lambda}_{m\pm1}=(T_{m_0},\boldsymbol{\lambda}_{m_\ell\pm1})$ with

$$\Delta = \beta_{m_0}(E_{\boldsymbol{\lambda}_{m_\ell \pm 1}} - E_{\boldsymbol{\lambda}_{m_\ell}}) - (f_{m_0,\ldots,m_\ell \pm 1,\ldots} - f_{m_0,\ldots,m_\ell,\ldots}), \tag{14}$$

where $\boldsymbol{\lambda}_{m_\ell \pm 1} = (\ldots, \lambda^{(\ell-1)}_{m_{\ell-1}}, \lambda^{(\ell)}_{m_\ell \pm 1}, \lambda^{(\ell+1)}_{m_{\ell+1}}, \ldots)$ and $\boldsymbol{\lambda}_{m_\ell} = (\ldots, \lambda^{(\ell-1)}_{m_{\ell-1}}, \lambda^{(\ell)}_{m_\ell}, \lambda^{(\ell+1)}_{m_{\ell+1}}, \ldots)$. Note that for the case of the function in Eq. (1), Eq. (14) becomes

$$\Delta = \beta_{m_0}(\lambda^{(\ell)}_{m_\ell \pm 1} - \lambda^{(\ell)}_{m_\ell}) V_\ell - (f_{m_0,\ldots,m_\ell \pm 1,\ldots} - f_{m_0,\ldots,m_\ell,\ldots}). \tag{15}$$

We remark that when MD simulations are performed in step 1 above, we also have to deal with the momenta $\boldsymbol{p}_k$, where $\boldsymbol{p}_k$ is the momentum of atom $k (k=1,\ldots,N)$, and the kinetic energy term should be included in the weight factor. When temperature $T_{m_0 \pm 1}$ is accepted for T-update in step 2, we rescale the momenta in the same way as in REMD,[24]

$$\boldsymbol{p}'_k = \sqrt{\frac{T_{m_0 \pm 1}}{T_{m_0}}} \boldsymbol{p}_k. \tag{16}$$

The kinetic energy terms then cancel out in Eq. (13) and we can use the same Δ [see Eqs. (13)–(15)] in the Metropolis criterion in step 2 for both MC and MD simulations.

Moreover, we remark that the random walk in β and in $\beta\lambda^{(\ell)}$ for the ST simulation corresponds to that in E_0 and in V_ℓ for the MUCA simulation,

$$E_0 \leftrightarrow \beta,$$

$$V_\ell \leftrightarrow \beta\lambda^{(\ell)} \quad (\ell = 1, \ldots, L). \tag{17}$$

They are in conjugate relation.

D. Multidimensional replica-exchange method

We now describe the MREM (Ref. 52). The system for the MREM consists of M noninteracting replicas of the original system in the "canonical ensemble" with $M (=M_0 \times M_1 \times \cdots \times M_L)$ different parameter sets $\boldsymbol{\Lambda}_m (m=1,\ldots,M)$, where $\boldsymbol{\Lambda}_m = (T_{m_0}, \lambda^{(1)}_{m_1}, \ldots, \lambda^{(L)}_{m_L})$ and $m_0 = 1,\ldots,M_0, m_\ell = 1,\ldots,M_\ell (\ell = 1,\ldots,L)$. Because the replicas are noninteracting, the weight factor is given by the product of Boltzmann-like factors for each replica:

$$W_{\mathrm{MREM}} \equiv \prod_{m_0=1}^{M_0} \prod_{m_1=1}^{M_1} \cdots \prod_{m_L=1}^{M_L} \exp(-\beta_{m_0} E_{\boldsymbol{\lambda}_m}). \tag{18}$$

REM closely follows the ST procedures described above. The multidimensional REM is realized by alternately performing the following two steps:

(1) For each replica, a canonical MC or MD simulation at the fixed parameter set is carried out simultaneously and independently for a certain steps.
(2) We exchange a pair of replicas i and j which are at the parameter sets $\boldsymbol{\Lambda}_m$ and $\boldsymbol{\Lambda}_{m+1}$, respectively. The transition probability for this replica-exchange process is given by

$$w(\boldsymbol{\Lambda}_m \leftrightarrow \boldsymbol{\Lambda}_{m+1}) = \min(1, \exp(-\Delta)), \tag{19}$$

where we have

$$\Delta = (\beta_{m_0} - \beta_{m_0+1})(E_{\boldsymbol{\lambda}_m}(q^{[j]}) - E_{\boldsymbol{\lambda}_m}(q^{[i]})) \tag{20}$$

for T-exchange, and

$$\Delta = \beta_{m_0}[(E_{\boldsymbol{\lambda}_{m_\ell+1}}(q^{[j]}) - E_{\boldsymbol{\lambda}_{m_\ell+1}}(q^{[i]})) - (E_{\boldsymbol{\lambda}_{m_\ell}}(q^{[j]}) - E_{\boldsymbol{\lambda}_{m_\ell}}(q^{[i]}))] \tag{21}$$

for $\lambda^{(\ell)}$-exchange (for one of $\ell = 1,\ldots,L$). Here, $q^{[i]}$ and $q^{[j]}$ stand for configuration variables for replicas i and j, respectively, before the replica exchange. For the case of the function in Eq. (1), Δ in Eq. (21) is given by

$$\Delta = \beta_{m_0}(\lambda^{(\ell)}_{m_\ell} - \lambda^{(\ell)}_{m_\ell+1})(V_\ell(q^{[j]}) - V_\ell(q^{[i]})). \tag{22}$$

We remark that when MD simulations are performed in step 1 above, we also have to deal with the momenta $\boldsymbol{p}_k$, where $\boldsymbol{p}_k$ is the momentum of atom $k (k=1,\ldots,N)$, and the kinetic energy term should be included in the weight factor. When the T-exchange between T_{m_0} of replica i and T_{m_0+1} of replica j is accepted in step 2, we rescale the momenta as follows:[24]

$$\boldsymbol{p}^{[i]\prime}_k = \sqrt{\frac{T_{m_0+1}}{T_{m_0}}} \boldsymbol{p}^{[i]}_k,$$

$$\boldsymbol{p}^{[j]\prime}_k = \sqrt{\frac{T_{m_0}}{T_{m_0+1}}} \boldsymbol{p}^{[j]}_k. \tag{23}$$

The kinetic energy terms then cancel out in Eq. (20) and we can use the same Δ [see Eqs. (20)–(22)] in the Metropolis criterion in step 2 for both MC and MD simulations.

Usually, M_0 and M_ℓ are taken to be even integers. The $M_0/2$ or $M_\ell/2$ pairs of replicas corresponding to neighboring T or $\lambda^{(\ell)}$ are simultaneously exchanged, and the pairing is alternated between the two possible choices, i.e., $((T_1,T_2),(T_3,T_4),\ldots)$ and $((T_2,T_3),(T_4,T_5),\ldots)$ or $((\lambda^{(\ell)}_1,\lambda^{(\ell)}_2),(\lambda^{(\ell)}_3,\lambda^{(\ell)}_4),\ldots)$ and $((\lambda^{(\ell)}_2,\lambda^{(\ell)}_3),(\lambda^{(\ell)}_4,\lambda^{(\ell)}_5),\ldots)$, respectively.

We also remark that we can easily generalize the (one-dimensional) multicanonical replica-exchange method[61–63] (MUCAREM) and simulated-tempering replica-exchange method[65] (STREM) to multidimensional ones. Here, MUCAREM is a REM where each replica corresponds to a MUCA ensemble with a finite energy range. For replica exchanges to occur, the neighboring MUCA ensembles are chosen so that they have overlapping energy distributions (for details, see Refs. 61–63). Likewise, STREM is a REM where each replica corresponds to a ST ensemble with a finite temperature range. For replica exchanges to occur, the neighboring ST ensembles are chosen so that they have overlapping temperature distributions (for details, see Ref. 65).

The multidimensional generalizations of MUCAREM and STREM can naturally be obtained by considering the following generalization:

$$E \to (E_0, V_1, \ldots, V_L),$$

$$T \to \mathbf{\Lambda} = (T, \lambda^{(1)}, \ldots, \lambda^{(L)}). \tag{24}$$

MUCAREM can be introduced to each or some of E_0 and $V_\ell (\ell = 1, \ldots, L)$ and STREM can be introduced to each or some of T and $\lambda^{(\ell)} (\ell = 1, \ldots, L)$. Namely, each replica of MUCAREM corresponds to MUCA ensemble with finite ranges of energy (chosen from $E_0, V_1, \ldots, V_L$) and each replica of STREM corresponds to ST ensemble with finite ranges of parameters (chosen from $T, \lambda^{(1)}, \ldots, \lambda^{(L)}$).

E. Weight factor determinations for multidimensional MUCA and ST

Among the three algorithms described above, only MREM can be performed without much preparation because the weight factor for MREM is just a product of regular Boltzmann-like factors. On the other hand, we do not know the MUCA and ST weight factors *a priori* and need to estimate them. We proposed a powerful method for the weight factor determination in the one-dimensional MUCA and ST.[61,71,62,63,65] In this method, we use a short REM simulation and the multiple-histogram reweighting techniques. Here, we present our general formulation of the new method for the multidimensional case (see also Refs. 4, 5, and 70).

Suppose we have made a single run of a short multidimensional REM simulation with $M (= M_0 \times M_1 \times \cdots \times M_L)$ replicas that correspond to M different parameter sets $\mathbf{\Lambda}_m (m = 1, \ldots, M)$. Let $N_{m_0, m_1, \ldots, m_L}(E_0, V_1, \ldots, V_L)$ and $n_{m_0, m_1, \ldots, m_L}$ be the $(L+1)$-dimensional potential energy histogram and the total number of samples obtained for the m-th parameter set $\mathbf{\Lambda}_m = (T_{m_0}, \lambda^{(1)}_{m_1}, \ldots, \lambda^{(L)}_{m_L})$, respectively. The generalized WHAM equations are then given by

$$n(E_0, V_1, \ldots, V_L) = \frac{\sum_{m_0, m_1, \ldots, m_L} N_{m_0, m_1, \ldots, m_L}(E_0, V_1, \ldots, V_L)}{\sum_{m_0, m_1, \ldots, m_L} n_{m_0, m_1, \ldots, m_L} \exp(f_{m_0, m_1, \ldots, m_L} - \beta_{m_0} E_{\mathbf{\lambda}_m})}, \tag{25}$$

and

$$\exp(-f_{m_0, m_1, \ldots, m_L}) = \sum_{E_0, V_1, \ldots, V_L} n(E_0, V_1, \ldots, V_L) \times \exp(-\beta_{m_0} E_{\mathbf{\lambda}_m}). \tag{26}$$

The density of states $n(E_0, V_1, \ldots, V_L)$ and the dimensionless free energy $f_{m_0, m_1, \ldots, m_L}$ are obtained by solving Eqs. (25) and (26) self-consistently by iteration. Namely, we can set all the $f_{m_0, m_1, \ldots, m_L}$ to, e.g., zero initially. We then use Eq. (25) to obtain $n(E_0, V_1, \ldots, V_L)$, which is substituted into Eq. (26) to obtain next values of $f_{m_0, m_1, \ldots, m_L}$, and so on. The weight factors for the multidimensional MUCA [see Eq. (5)] and the multidimensional ST [see Eqs. (9) and (11)] are then obtained from the generalized density of states $n(E_0, V_1, \ldots, V_L)$ and the dimensionless free energy $f_{m_0, m_1, \ldots, m_L}$, respectively.

We remark that for complex systems, the MUCA or ST simulation with the MUCA or ST weight factor obtained by the above method is often insufficient. In such cases, we can iterate the multidimensional MUCA or ST simulation in which the estimate of the multidimensional MUCA or ST weight factor is updated by the single- or multiple-histogram reweighting techniques, respectively.[63] To be more specific, this iterative process can be summarized as follows. The MUCA production run corresponds to a MUCA simulation with the weight factor $W_{\mathrm{MU}}(E_0, V_1, \ldots, V_L)$. Let $N_{\mathrm{MU}}(E_0, V_1, \ldots, V_L)$ be the histogram of the distribution $P_{\mathrm{MU}}(E_0, V_1, \ldots, V_L)$ of $E_0, V_1, \ldots, V_L$, obtained by the production run. The new estimate of the density of states $n(E_0, V_1, \ldots, V_L)$ can be given by the single-histogram reweighting techniques as follows [see Eq. (4)]:

$$n(E_0, V_1, \ldots, V_L) = \frac{N_{\mathrm{MU}}(E_0, V_1, \ldots, V_L)}{W_{\mathrm{MU}}(E_0, V_1, \ldots, V_L)}. \tag{27}$$

On the other hand, the ST production run corresponds to a ST simulation with the weight factor $W_{\mathrm{ST}}(\mathbf{\Lambda})$. From this ST production run, we obtain $N_{m_0, m_1, \ldots, m_L}(E_0, V_1, \ldots, V_L)$ and $n_{m_0, m_1, \ldots, m_L}$ in Eq. (25). The improved dimensionless free energy can be obtained by the multiple-histogram reweighting techniques of Eqs. (25) and (26). The improved density of states and the dimensionless free energy lead to a new MUCA weight factor and a new ST weight factor. The results of this production run may yield optimal MUCA and ST weight factors that give sufficiently flat energy and parameter distributions for the entire energy and parameter ranges of interest, respectively. If not, we can repeat the above process by obtaining the third estimate of the MUCA and ST weight factors by a MUCA and ST production run, and so on.

Moreover, we can iterate the multidimensional MUCAREM and STREM which were described at the end of Sec. II D using the multiple-histogram reweighting techniques, and obtain accurate multidimensional MUCA and ST weight factors as in the case for the one-dimensional case.[63]

F. Averages of physical quantities

In this subsection, we present the equations to calculate ensemble averages of physical quantities with any temperature T and any parameter $\boldsymbol{\lambda}$ values. The expectation values of a physical quantity A at any $T(=1/k_B\beta)$ and any $\boldsymbol{\lambda}$ is given by

$$\langle A\rangle_{T,\boldsymbol{\lambda}} = \frac{\sum_{E_0,V_1,\ldots,V_L} A(E_0,V_1,\ldots,V_L)n(E_0,V_1,\ldots,V_L)\exp(-\beta E_{\boldsymbol{\lambda}})}{\sum_{E_0,V_1,\ldots,V_L} n(E_0,V_1,\ldots,V_L)\exp(-\beta E_{\boldsymbol{\lambda}})}. \tag{28}$$

For the multidimensional MUCA simulation with the weight factor $W_{\mathrm{MU}}(E_0,\ldots,V_L)$, the best estimate of the density of states $n(E_0,V_1,\ldots,V_L)$ can be given by the single-histogram reweighting techniques [see Eq. (27)]. By substituting this quantity into Eq. (28), one can calculate the ensemble average of the physical quantity A as functions of T and $\boldsymbol{\lambda}$. Moreover, the ensemble average of the physical quantity A [including those that cannot be expressed as a function of E_0 and $V_\ell(\ell=1,\ldots,L)$] can be obtained as long as one stores the "trajectory" x_k from the production run, namely, we have

$$\langle A\rangle_{T,\boldsymbol{\lambda}} = \frac{\sum_{x_k} A(x_k)W_{\mathrm{MU}}^{-1}(E_0(x_k),\ldots,V_L(x_k))\exp(-\beta E_{\boldsymbol{\lambda}}(x_k))}{\sum_{x_k} W_{\mathrm{MU}}^{-1}(E_0(x_k),\ldots,V_L(x_k))\exp(-\beta E_{\boldsymbol{\lambda}}(x_k))}. \tag{29}$$

Here, x_k is the configuration at the kth MC (or MD) step.

For the multidimensional ST or REM simulation, an ensemble average of the physical quantity A at any T and any $\boldsymbol{\lambda}$ is given by the multiple-histogram reweighting techniques as follows. In the ST or the REM simulation, we first obtain $N_{m_0,m_1,\ldots,m_L}(E_0,V_1,\ldots,V_L)$ and $n_{m_0,m_1,\ldots,m_L}$ in Eq. (25). The density of states $n(E_0,V_1,\ldots,V_L)$ and the dimensionless free energy $f_{m_0,m_1,\ldots,m_L}$ can then be obtained by solving Eqs. (25) and (26) self-consistently by iteration. Substituting the obtained density of states $n(E_0,V_1,\ldots,V_L)$ into Eq. (28), one can calculate the ensemble average of the physical quantity A at any T and any $\boldsymbol{\lambda}$.

Moreover, the ensemble average of the physical quantity A [including those that cannot be expressed as functions of E_0 and $V_\ell(\ell=1,\ldots,L)$] can be obtained from the trajectory of configurations of the production run.[62] Namely, we first obtain $f_{m_0,m_1,\ldots,m_L}$ for each $(m_0=1,\ldots,M_0,m_1=1,\ldots,M_1,\ldots,m_L=1,\ldots,M_L)$ by solving Eqs. (25) and (26) self-consistently, and then we have

$$\langle A\rangle_{T,\boldsymbol{\lambda}} = \frac{\sum_{m_0=1}^{M_0}\cdots\sum_{m_L=1}^{M_L}\sum_{x_m} A(x_m)\dfrac{\exp(-\beta E_{\boldsymbol{\lambda}}(x_m))}{\sum_{n_0=1}^{M_0}\cdots\sum_{n_L=1}^{M_L} n_{n_0,\ldots,n_L}\exp(f_{n_0,\ldots,n_L}-\beta_{n_0}E_{\boldsymbol{\lambda}_n}(x_m))}}{\sum_{m_0=1}^{M_0}\cdots\sum_{m_L=1}^{M_L}\sum_{x_m}\dfrac{\exp(-\beta E_{\boldsymbol{\lambda}}(x_m))}{\sum_{n_0=1}^{M_0}\cdots\sum_{n_L=1}^{M_L} n_{n_0,\ldots,n_L}\exp(f_{n_0,\ldots n_L}-\beta_{n_0}E_{\boldsymbol{\lambda}_n}(x_m))}}, \tag{30}$$

where x_m are the configurations obtained at $\Lambda_m=(T_{m_0},\lambda_m)=(T_{m_0},\lambda_{m_1}^{(1)},\cdots,\lambda_{m_L}^{(L)})$. Here, the trajectories x_m are stored for each Λ_m separately.

III. COMPUTATIONAL DETAILS

We tested the effectiveness of the new algorithms by using a system of a 17-residue fragment of ribonuclease T_1. It is known by experiments that this peptide fragment forms α-helical conformations.[76] The amino-acid sequence is SSDVSTAQIAAYKLHED, which is the part from residue Ser-13 through Asp-29 with the mutations A21I and G23A from the native sequence.[76] We have performed a two-dimensional REM simulation and a two-dimensional ST simulation. In these simulations, we used the following energy function:

$$E_\lambda = E_0 + \lambda E_{\mathrm{sol}}, \tag{31}$$

where we set $L=1$, $V_1=E_{\mathrm{sol}}$, and $\lambda^{(1)}=\lambda$ in Eq. (1). Here, E_0 is the potential energy of the solute and E_{sol} is the solvation free energy. The parameters in the conformational energy as

TABLE I. Acceptance ratios of replica exchanges between pairs of temperatures, (T_{m_0}, T_{m_0+1}), $(m_0=1,\ldots,8)$, with fixed $\lambda_{m_1}(m_1=1,\ldots,4)$ from the two-dimensional REM simulation. In the case of $m_0=8$, T_{m_0+1} is set to be T_1.

	(T_1,T_2)	(T_2,T_3)	(T_3,T_4)	(T_4,T_5)	(T_5,T_6)	(T_6,T_7)	(T_7,T_8)	(T_8,T_1)
λ_1	0.539	0.516	0.476	0.393	0.278	0.229	0.338	0.000
λ_2	0.457	0.443	0.436	0.422	0.290	0.206	0.355	0.000
λ_3	0.491	0.490	0.479	0.408	0.211	0.229	0.448	0.000
λ_4	0.495	0.478	0.450	0.306	0.177	0.339	0.496	0.000

well as the molecular geometry were taken from ECEPP/2.[77–79] The dielectric constant ϵ was set equal to 2 according to the ECEPP prescription. The backbone was terminated by a neutral NH_2-group and a neutral-COOH group at the N-terminus and at the C-terminus, respectively.

The solvation term $E_{\rm sol}$ is given by the sum of terms that are proportional to the solvent-accessible surface area of heavy atoms of the solute,[80]

$$E_{\rm sol} = \sum_i \sigma_i S_i, \tag{32}$$

where the summation extends over all heavy atoms i (here, the number of the heavy atoms is 129), and S_i is the corresponding solvent-accessible surface area. For these area calculations, the heavy atoms containing hydrogen atoms are treated as "united atoms." The constant of proportionality σ_i represents the contribution to the solvation free energy of heavy atoms i per unit accessible surface area. In the present work, we used the parameters of Ref. 80 (there are only six different values of σ for the heavy atoms). The accessible surface area S_i is obtained by the surface area of fused spheres centered at each united atom. The radius of the sphere is R_i+R_w, where R_w is the effective radius of the solvent molecule. Here, we set R_i to van der Waals radius and R_w to 1.4 Å. For the calculation of solvent-accessible surface area, we used the computer code NSOL.[81]

The computer code KONF90 (Refs. 82 and 83) was modified in order to accommodate the generalized-ensemble algorithms. The peptide-bond dihedral angles ω were fixed at the value 180° for simplicity. The dihedral angles ϕ and ψ in the main chain and χ in the side chains constituted the variables to be updated in the simulations. The number of degrees of freedom for the peptide is thus 80. One MC sweep consists of updating all these angles once with Metropolis evaluation[75] for each update. The simulations were started from randomly generated conformations. We prepared eight temperatures $(M_0=8)$ which are distributed exponentially between $T_1=300$ K and $T_{M_0}=700$ K (i.e., 300.00, 338.60, 382.17, 431.36, 486.85, 549.49, 620.20, and 700.00 K) and four equally spaced λ values $(M_1=4)$ ranging from 0 to 1 (i.e., $\lambda_1=0$, $\lambda_2=1/3$, $\lambda_3=2/3$, and $\lambda_4=1$) in the two-dimensional REM simulation and the two-dimensional ST simulation. Simulations with $\lambda=0$ (i.e., $E_\lambda=E_0$) and with $\lambda=1$ (i.e., $E_\lambda=E_0+E_{\rm sol}$) correspond to those in gas phase and in aqueous solution, respectively.

In the present article, the canonical expectation value of a physical quantity A at T_{m_0} and $\lambda_{m_1}(m_0=1,\ldots,8;m_1=1,\ldots,4)$ was calculated by the usual arithmetic mean as follows:

$$\langle A\rangle_{T_{m_0},\lambda_{m_1}} = \frac{1}{n_{m_0,m_1}} \sum_{k=1}^{n_{m_0,m_1}} A(x_{m_0,m_1}(k)), \tag{33}$$

where $x_{m_0,m_1}(k)(k=1,\ldots,n_{m_0,m_1})$ are the configurations obtained at T_{m_0} and λ_{m_1} and n_{m_0,m_1} is the total number of measurements made at T_{m_0} and λ_{m_1}. For the expectation values at any other values of T and λ, we can use the WHAM techniques [namely, Eqs. (25), (26), and (30)].

IV. RESULTS AND DISCUSSION

A. Two-dimensional REM simulation

We first present the results of the two-dimensional REM simulation. We used 32 replicas with the eight temperature values and the four λ values given above. Before taking the data, we made the two-dimensional REM simulation of 100 000 MC sweeps with each replica for thermalization. We then performed the two-dimensional REM simulation of 1 000 000 MC sweeps for each replica to determine the weight factor for the two-dimensional ST simulation. At every 20 MC sweeps, either T-exchange or λ-exchange was tried (the choice of T or λ was made randomly). In each case, either set of pairs of replicas $((1,2),\ldots,(M-1,M))$ or

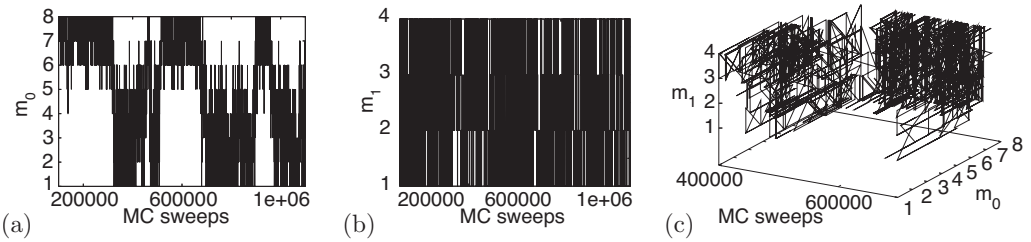

FIG. 1. Time series of the labels of T_{m_0}, m_0, (a) and λ_{m_1}, m_1, (b) as functions of MC sweeps, and that of both T_{m_0} and λ_{m_1} for the region from 400 000 MC sweeps to 700 000 MC sweeps (c). The results were from one of the replicas (replica 1). In (a) and (b), MC sweeps start at 100 000 and end at 1 100 000 because the first 100 000 sweeps have been removed from the consideration for thermalization purpose.

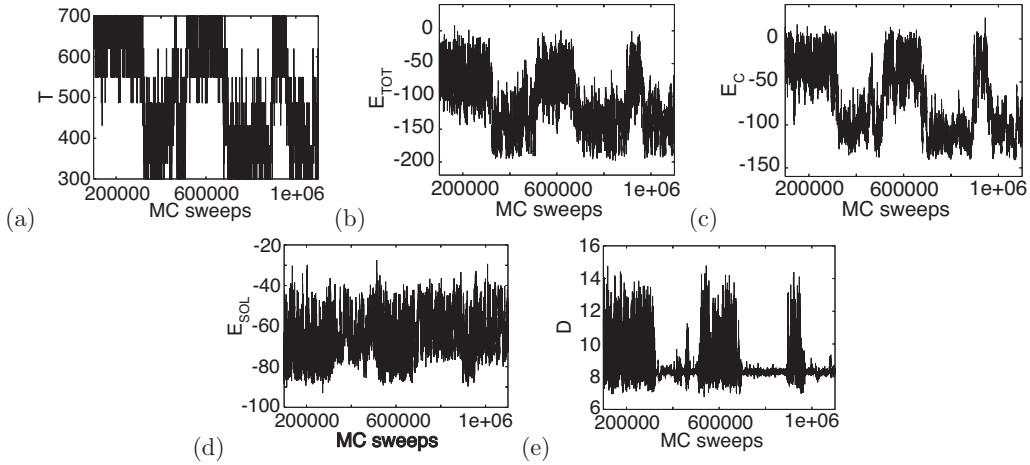

FIG. 2. Time series of the temperature T (a), total energy E_{tot} (b), conformational energy E_C (c), solvation free energy E_{sol} (d), and end-to-end distance D (e) for the same replica as in Fig. 1. The temperature is in K, the energy is in kcal/mol, and the end-to-end distance is in Å.

$((2,3),\ldots,(M,1))$ was also chosen randomly, where M is M_0 and M_1 for T-exchange and λ-exchange, respectively.

In Table I, we list the acceptance ratios of replica exchanges between pairs of temperatures with fixed λ in the two-dimensional REM simulation. Although we tried T-exchange between T_8 and T_1, they did not occur (see Table I). Except for this case, the acceptance ratios of replica exchanges ranged between 0.177 and 0.539 and T-exchanges occurred frequently. The results suggest that the simulation realized a random walk in temperature space. In Table II, we list the acceptance ratios of replica exchanges between pairs of λ values with fixed temperatures. Although the acceptance ratios of λ-exchanges were not as uniform as in the T-exchange case, they were all sufficiently large. The random walk in λ space was also realized in the simulation.

In Fig. 1 we show the time series of labels of T_{m_0} (i.e., m_0) and λ_{m_1} (i.e., m_1) for one of the replicas. The replica realized a random walk not only in temperature space but also in λ space. The behavior of T and λ for other replicas was also similar (data not shown). From Fig. 1, one finds that the λ-random walk is more frequent than the T-random walk.

We also show the time series of temperature T, total energy E_{tot}, conformational energy E_C, solvation free energy E_{sol}, and end-to-end distance D for the same replica in Fig. 2. Here, the end-to-end distance is defined as the distance between the nitrogen atom of backbone in N-terminus and the oxygen atom of backbone in C-terminus. In the previous REM simulation that covered the temperature range between 250 and 700 K in aqueous solution[63] (which corresponds to the present system with $\lambda=1$), the values of the total energy ranged from about −190 to about −170 kcal/mol and from about −115 to −70 kcal/mol at 294.15 and 700 K, respectively. It was also shown that while the global-minimum-energy conformation at 250 K was a complete α-helix structure (with total energy value −200 kcal/mol), the conformations at high temperatures were random coils. In the present simulation, the total energy covered an energy range from −200 to −10 kcal/mol [see Fig. 2(b)], which covered a slightly wider energy range than that of the previous simulation.[63] From Figs. 2(a) and 2(e), we find that at lower temperatures the end-to-end distance is about 8 Å, which is the length of a fully α-helical conformation and that at higher temperatures it fluctuates much for a range from 7 to 14 Å. It suggests that α-helix structures exist at low temperatures and random-coil structures occur at high temperatures. There are transitions from/to α-helix structures to/from random coils during the simulation. It indicates that the REM simulation avoided getting trapped in local-minimum-energy states and sampled a wide configurational space.

We remark that the conformational energy tends to increase and the solvation free energy tends to decrease as the temperature increases [see Figs. 2(a), 2(c), and 2(d)]. (The behavior of the solvation free energy is not as clear as that of the conformational energy, but it is more clearly shown in Fig. 10 below.) At high temperatures, random-coil structures, which have high conformational energy, were dominant be-

TABLE II. Acceptance ratios of replica exchanges between pairs of λ parameters, $(\lambda_{m_1},\lambda_{m_1+1})$, $(m_1=1,\ldots,4)$, with fixed temperatures $T_{m_0}(m_0=1,\ldots,8)$ from the two-dimensional REM simulation. In the case of $m_1=4$, λ_{m_1+1} is set to be λ_1.

	(λ_1,λ_2)	(λ_2,λ_3)	(λ_3,λ_4)	(λ_4,λ_1)
T_1	0.108	0.340	0.593	0.669
T_2	0.114	0.391	0.548	0.616
T_3	0.116	0.387	0.593	0.813
T_4	0.139	0.468	0.759	0.958
T_5	0.345	0.585	0.679	0.489
T_6	0.396	0.541	0.624	0.489
T_7	0.393	0.585	0.824	0.489
T_8	0.475	0.749	0.971	0.492

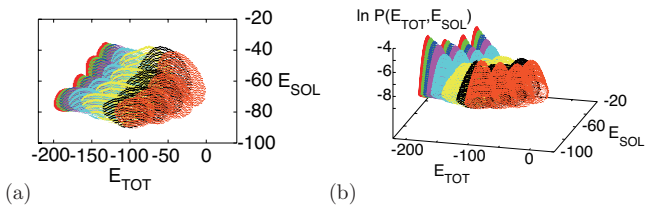

FIG. 3. (Color) Contour curves and histograms of distributions of the total energy E_{tot} and the solvation free energy E_{sol} [(a) and (b)] from the two-dimensional REM simulation.

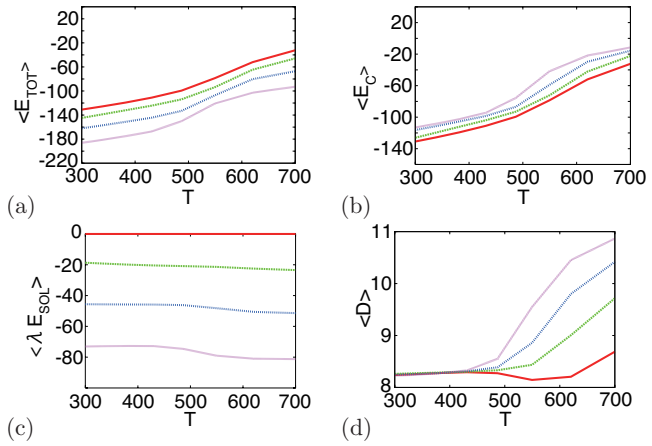

FIG. 4. (Color) The average total energy (a), average conformational energy (b), average of $\lambda \times E_{sol}$ (c), and average end-to-end distance (d) with all the λ values as functions of temperature. The lines colored in red, green, blue, and purple are for λ_1, λ_2, λ_3, and λ_4, respectively.

cause of the conformational entropic effects. In addition, these random structures had lower solvation free energy because the atoms in them were more exposed to solvent than those in compact structures obtained at low temperatures.

The canonical probability distributions of E_{tot} and E_{sol} at the 32 conditions obtained from the two-dimensional REM simulation are shown in Fig. 3. For an optimal performance of the REM simulation, there should be enough overlaps between all pairs of neighboring distributions, which will lead to sufficiently uniform and large acceptance ratios of replica exchanges. There are indeed ample overlaps between the neighboring distributions in Fig. 3.

The average total energy, average conformational energy, average solvation free energy multiplied by λ, and average end-to-end distance as functions of temperature are shown in Fig. 4. The average quantities were calculated by Eq. (33). The shapes of the total energy as a function of temperature are sigmoidal. There exist helix-coil transitions in the system.[63] The transition temperature is obtained by the peak in the specific heat or the derivative of the total energy. From Fig. 4(a), we find that the transition temperature is about 530 K in aqueous solution as in the previous REM simulation and about 580 K in gas phase. This implies that the helical structures are unfolded more easily in aqueous solution than in gas phase.[84,85] We remark that these transition temperatures are unphysically high because our energy functions are not accurate enough to give quantitative temperature values. The average end-to-end distance also suggests the existence of helix-coil transitions [see Fig. 4(d)].

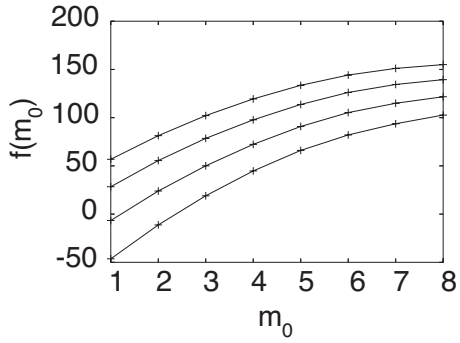

FIG. 5. The dimensionless free energy f_{m_0,m_1} as a function of labels of temperature, m_0, obtained by the two-dimensional REM simulation. The four curves correspond to $m_1=1,2,3$, and 4 from top to bottom.

B. Two-dimensional ST simulation

We now use the results of the two-dimensional REM simulation to determine the weight factors for the two-dimensional ST simulation by the multiple-histogram reweighting techniques. Namely, by solving the generalized WHAM equations in Eqs. (25) and (26) with the obtained histograms at the 32 conditions (see Fig. 3), we obtained 32 values of the ST parameters $f_{m_0,m_1}(m_0=1,\ldots,8;m_1=1,\ldots,4)$. In Fig. 5, we show the obtained f_{m_0,m_1} as functions of the temperature label m_0. With fixed m_1 values, the dimensionless free energy f_{m_0,m_1} monotonically increases as a function of m_0.

After obtaining the ST weight factors, $W_{ST}=\exp(-\beta_{m_0}(E_C+\lambda_{m_1}E_{sol})+f_{m_0,m_1})$, we carried out the two-dimensional ST simulation of 1 000 000 MC sweeps for data collection after 100 000 MC sweeps for thermalization. At every 20 MC sweeps, either T_{m_0} or λ_{m_1} was updated to $T_{m_0\pm1}$ or $\lambda_{m_1\pm1}$, respectively (the choice of T or λ update and the choice of ±1 were made randomly).

In Tables III and IV, we list the acceptance ratios of T- and λ-updates, respectively. Although we tried the T-updates between T_1 and T_8, the trials were rejected. Except for this case, the acceptance ratios for T-updates ranged from 0.28 to 0.66 and T-updates occurred frequently. The results suggest that a T-random walk was realized in the simulation. In Table IV, there were few λ-updates between λ_1 and λ_4. Except for this special case, the acceptance ratios for λ-updates ranged from 0.15 to 0.63. A random walk in λ space was also realized in the simulation.

In Fig. 6, we show the time series of the labels of T_{m_0} and λ_{m_1} (namely, m_0 and m_1). A random walk not only in temperature space but also in λ space was realized in the

TABLE III. Acceptance ratios of T-updates, $T_{m_0}\rightarrow T_{m_0\pm1}(m_0=1,\ldots,8)$, with fixed $\lambda_{m_1}(m_1=1,\ldots,4)$ in the two-dimensional ST simulation. In the cases of $m_0=1$ and 8, T_{m_0-1} and T_{m_0+1} are set to be T_8 and T_1, respectively.

T_{m_0}	T_1		T_2		T_3		T_4		T_5		T_6		T_7		T_8	
$T_{m_0\pm1}$	T_8	T_2	T_1	T_3	T_2	T_4	T_3	T_5	T_4	T_6	T_5	T_7	T_6	T_8	T_7	T_1
λ_1	0.00	0.63	0.60	0.62	0.61	0.57	0.59	0.55	0.56	0.43	0.47	0.34	0.44	0.46	0.48	0.00
λ_2	0.00	0.59	0.66	0.57	0.65	0.56	0.62	0.56	0.58	0.43	0.51	0.36	0.37	0.54	0.54	0.00
λ_3	0.00	0.60	0.66	0.63	0.62	0.57	0.57	0.53	0.53	0.38	0.40	0.37	0.44	0.59	0.57	0.00
λ_4	0.00	0.58	0.64	0.62	0.60	0.57	0.57	0.43	0.49	0.28	0.32	0.45	0.46	0.61	0.58	0.00

TABLE IV. Acceptance ratios of λ-updates, $\lambda_{m_1} \rightarrow \lambda_{m_1 \pm 1} (m_1 = 1, \ldots, 4)$, with fixed $T_{m_0} (m_0 = 1, \ldots, 8)$ in the two-dimensional ST simulation. In the cases of $m_1 = 1$ and 4, $\lambda_{m_1 - 1}$ and $\lambda_{m_1 + 1}$ are set to be λ_4 and λ_1, respectively.

λ_{m_1}	λ_1		λ_2		λ_3		λ_4	
$\lambda_{m_1 \pm 1}$	λ_4	λ_2	λ_1	λ_3	λ_2	λ_4	λ_3	λ_1
T_1	0.00	0.21	0.24	0.15	0.19	0.43	0.46	0.00
T_2	0.00	0.29	0.28	0.19	0.27	0.45	0.46	0.00
T_3	0.00	0.25	0.28	0.28	0.34	0.49	0.52	0.00
T_4	0.01	0.32	0.32	0.36	0.41	0.54	0.54	0.01
T_5	0.03	0.33	0.32	0.44	0.40	0.53	0.55	0.03
T_6	0.01	0.38	0.38	0.41	0.43	0.43	0.52	0.01
T_7	0.02	0.31	0.34	0.46	0.42	0.51	0.58	0.03
T_8	0.04	0.37	0.39	0.57	0.52	0.63	0.62	0.05

simulation, as expected. We find that the λ-random walk is more frequent than the T-random walk [compare Figs. 6(a) and 6(b)]. In Fig. 7, the histogram of the distributions of m_0 and m_1 is shown. The histogram was flat for wide ranges of both T and λ. The two-dimensional ST simulation was thus successful in the sense that the updates of T and λ occurred frequently and that all values of both T and λ distributed almost uniformly.

We show the time series of temperature T, total energy E_{tot}, conformational energy E_C, solvation free energy E_{sol}, and end-to-end distance D from the two-dimensional ST simulation in Fig. 8. The results are all similar to those from the two-dimensional REM simulation in Fig. 2. The random walk both in T space and in λ space induced that both in conformational energy space and in solvation free energy space. From the results of the single two-dimensional ST simulation run, we calculated average values of physical quantities by Eq. (33). We show the average total energy, average conformational energy, average $\lambda \times E_{\mathrm{sol}}$, and average end-to-end distance in Fig. 9. The results are in good agreement with those of the REM simulation in Fig. 4.

We find that the results of the two-dimensional ST simulation are in complete agreement with those of the two-dimensional REM simulation for the average quantities. The only difference between the two simulations is the number of replicas. In the present simulation, while the REM simulation used 32 replicas, the ST simulation used only one replica. Hence, we can save much computer power with ST.

C. Detailed analysis of the solvent effects

In this subsection, we discuss the results of the simulations in detail with respect to the solvent effects. We found in the previous subsections that the results of both REM and ST simulations were essentially identical. Thus, in the following, we describe only the results of the two-dimensional REM simulation because it had 32 times more data than the ST case. To investigate the dependence on the values of T and λ, we separately show the time series of the total energy E_{tot}, conformational energy E_C, solvation free energy E_{sol} with two λ values (λ_1 or λ_4), and three T values (T_1, T_6, and T_8) in Fig. 10. Here, in gas phase, the solvation free energy E_{sol} was calculated only for the purpose of comparisons and does not contribute to the total energy E_{tot} (i.e., $E_{\mathrm{tot}} = E_C$) [E_{tot} in Fig. 10(a) has the same value as E_C in Fig. 10(c)]. The values of the total energy at 300 and 700 K in aqueous solution [Fig. 10(b)] were around −180 and −90 kcal/mol, respectively. The results agree with those in the previous (one-dimensional) REM simulation in aqueous solution.[63] The total energy in gas phase [Fig. 10(a)] also covered a wide energy range from −140 to 0 kcal/mol. From Fig. 10, we find that there are different behaviors of energy terms between in gas phase and in aqueous solution. For all the temperatures, while the conformational energy E_C in aqueous solution [Fig. 10(d)] was slightly higher than that in gas phase [Fig. 10(c)], the solvation free energy E_{sol} in aqueous solution [Fig. 10(f)] was lower than that in gas phase [Fig. 10(e)]. In gas phase, the system is affected only by the conformational energy; on the other hand, in aqueous solution, the system receives effects from both the conformational energy and the solvation free energy. There is a competition between E_C and E_{sol} in aqueous solution. Thus, the conformational energy in aqueous solution is slightly higher than that in gas phase to adjust between E_C and E_{sol}.

We compare the conformations obtained with $\lambda = 0$ (in

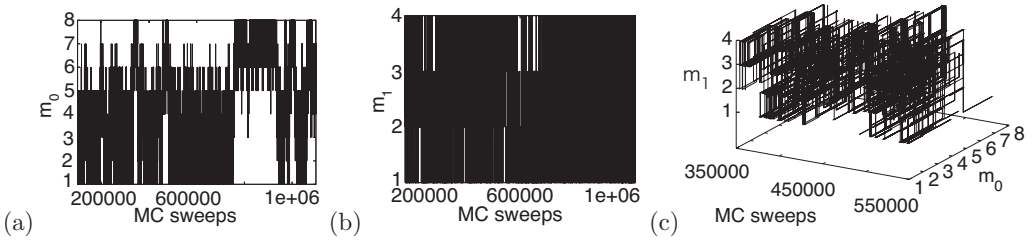

FIG. 6. Time series of the labels of T_{m_0}, i.e., m_0 (a) and λ_{m_1}, i.e., m_1 (b) as functions of MC sweeps, and those of both T_{m_0} and λ_{m_1} for the region from 350 000 MC sweeps to 550 000 MC sweeps (c). In (a) and (b), MC sweeps start at 100 000 and end at 1 100 000 because the first 100 000 sweeps have been removed from the consideration for thermalization.

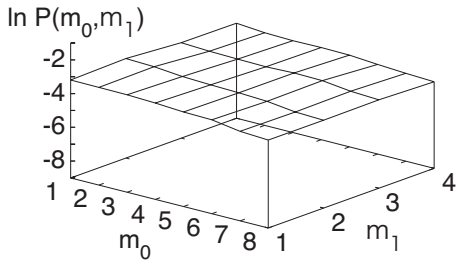

FIG. 7. Histogram of the distribution of the labels of T_{m_0}, m_0, and λ_{m_1}, m_1, obtained by the two-dimensional ST simulation.

gas phase) and those with $\lambda=1$ (in aqueous solution) at the lowest temperature (300 K). Most conformations were complete α-helix structures in both cases for all the MC sweeps (data not shown). In particular, we compare the lowest-total-energy conformation in gas phase with that in aqueous solution. The total energy, conformational energy, and solvation free energy of the lowest-total-energy conformation in gas phase were -148.43, -148.43, and -44.93 kcal/mol, respectively. On the other hand, the total energy, conformational energy, and solvation free energy of the lowest-total-energy conformation in aqueous solution were -203.68, -133.90, and -69.78 kcal/mol, respectively. We find that the energy values of the two conformations are typical ones at 300 K in Fig. 10. The results confirm the validity to use both the lowest-total-energy conformations to clarify the difference between in gas phase and in aqueous solution at 300 K. The lowest-total-energy conformations are shown in Fig. 11. Both conformations were complete α-helix structures. The backbones of the two conformations are essentially identical. However, some side-chain conformations are different. We show the values of the "atomistic" solvation free energy $E_{\mathrm{sol}i}$ of heavy atoms i [here, $E_{\mathrm{sol}i}=\sigma_i S_i$ in Eq. (32)] of the two lowest-total-energy conformations in Fig. 12. There were some heavy atoms with large differences in the atomistic solvation free energy between in gas phase and in aqueous solution. We list the values of the differences in the atomistic solvent-accessible surface area $(\Delta S_i=S_i(\mathrm{sol})-S_i(\mathrm{gas}))$ and the atomistic solvation free energy $(\Delta E_{\mathrm{sol}i}=E_{\mathrm{sol}i}(\mathrm{sol})-E_{\mathrm{sol}i}(\mathrm{gas}))$ of the nine heavy atoms of which the absolute values of $\Delta E_{\mathrm{sol}i}$ are larger than 1.2 kcal/mol in Table V. The nine heavy atoms are the atoms of N in Ser1, OG in Ser1, OG in Ser2, OD in Asp3, NE in Gln8, OH in Tyr12, NZ in Lys13, OE in Glu16, and OD in Asp17. (The numbers here correspond to the residue numbers in the peptide fragment. For instance, Ser1 and Asp17 correspond to Ser-13 and Asp-29 of the native sequence of ribonuclease T_1.) We show these heavy atoms with van der Waals representation in Fig. 11(c) (where the oxygen atoms are colored in red and the nitrogen atoms are colored in blue). The differences in the total accessible surface area $[\Delta S=S(\mathrm{sol})-S(\mathrm{gas})]$ and the total solvation free energy $[\Delta E_{\mathrm{sol}}=E_{\mathrm{sol}}(\mathrm{sol})-E_{\mathrm{sol}}(\mathrm{gas})]$ of the lowest-total-energy conformations between in gas phase and in aqueous solution were 99.74 Å^2 and -24.85 kcal/mol, respectively. The atoms located on the side chains can make hydrogen bonds with water molecules. The heavy atoms preferred to make interactions with water atoms because the atomistic solvation free energy decreased as the accessible surface area increased. The arrangements of side chains of the heavy atoms occurred in aqueous solution so that their accessible surface areas increased (i.e., to expose to water). It implies that at low temperatures, a random walk in λ space causes the change of side-chain structures because of the solvent effects, while the backbone remains almost identical (α-helix structure).

Moreover, we compare the conformations with $\lambda=0$ (in gas phase) and those with $\lambda=1$ (in aqueous solution) at the highest temperature T_8. The snapshots of the conformations at 200 000 MC sweeps, 600 000 MC sweeps, and 1 000 000 MC sweeps in gas phase and in aqueous solution are shown in Fig. 13. The corresponding time series of the end-to-end distance are also shown in Fig. 14. Although all structures are extended and in random-coil state due to entropic effects, there are different characteristics of the conformations in gas phase and in aqueous solution. The conformations in gas phase seem to be slightly more compact than those in aqueous solution. The end-to-end distance in gas phase was also smaller than that in aqueous solution. In aqueous solution, charged atoms prefer to make interactions with water molecules and thus there are less intrachain interactions. As a

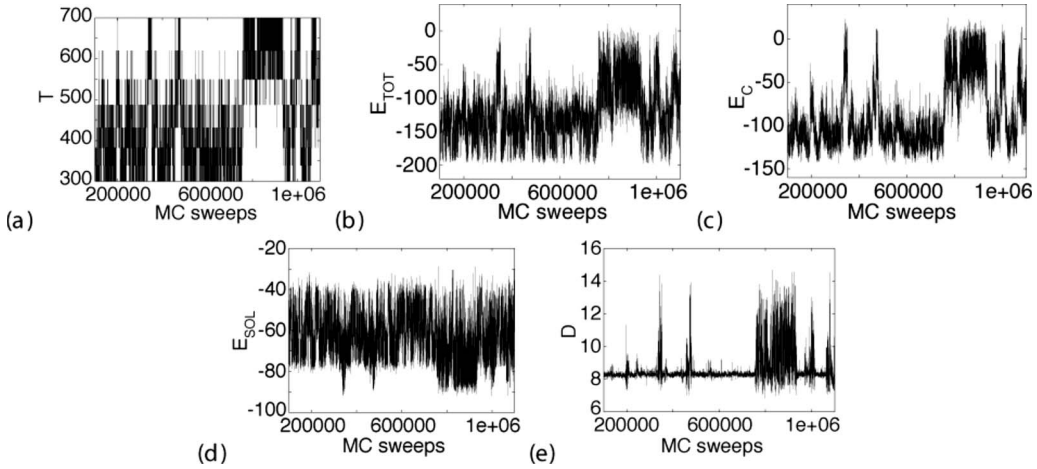

FIG. 8. Time series of the temperature (a), total energy (b), conformational energy (c), solvation free energy (d), and end-to-end distance D (e) for the two-dimensional ST simulation.

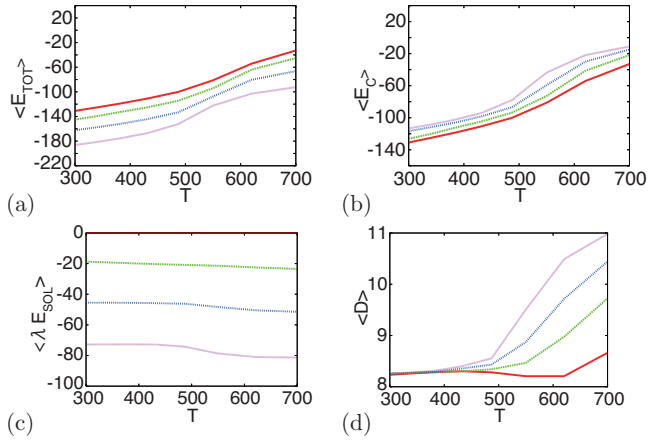

FIG. 9. (Color) The average total energy (a), average conformational energy (b), average of $\lambda \times E_{sol}$ (c), and average end-to-end distance (d) with all the λ values as functions of temperature. The lines colored in red, green, blue, and purple are for λ_1, λ_2, λ_3, and λ_4, respectively.

result, the conformations in aqueous solution are more extended than those in gas phase at the same temperature. These results are also supported by the behavior of the solvation free energy in Fig. 9(a) and the end-to-end distance in Fig. 9(d). At high temperatures, it implies that both structures are random coils but a random walk of λ space causes to change structures from/to a slightly compact ones to/from extended ones.

V. CONCLUSIONS

In this article we presented the general formulations of the multidimensional MUCA, ST, and REM. We generalized

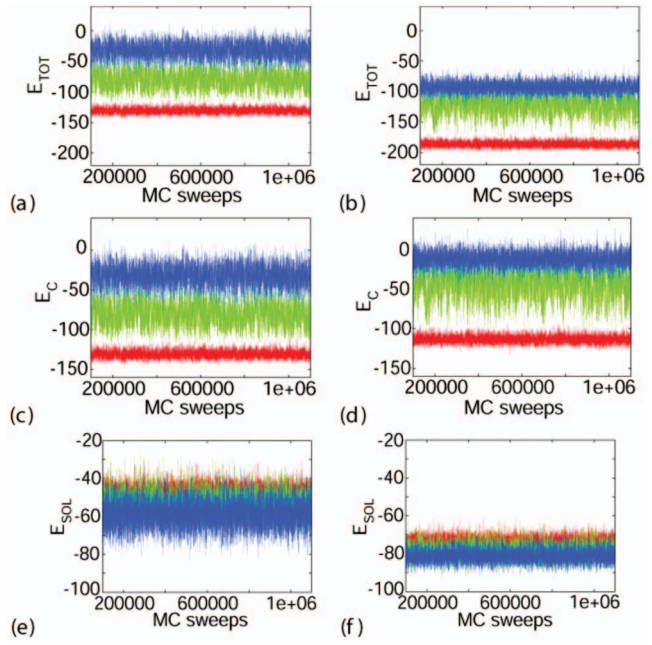

FIG. 10. (Color) Time series of the total energy [(a) and (b)], conformational energy [(c) and (d)], and solvation free energy [(e) and (f)] with $\lambda=0$ (in gas phase) and with $\lambda=1$ (in aqueous solution), respectively. The red, green, and blue curves are for the fixed temperatures T_1 (300 K), T_6 (549 K), and T_8 (700 K), respectively. In gas phase, the total energy of (a) is the same as the conformational energy of (c). The scales of the ordinate in (a) and (c) are different from each other.

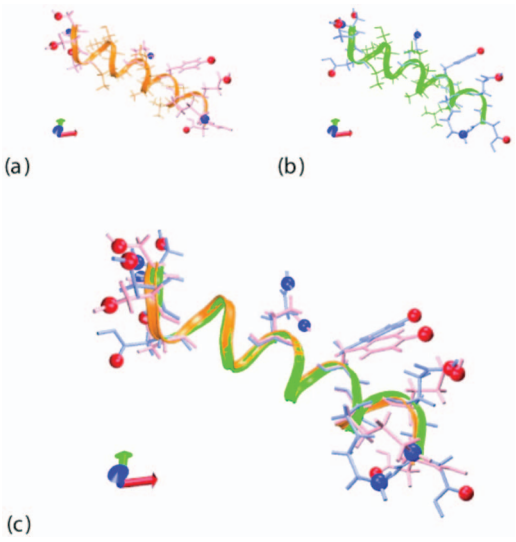

FIG. 11. (Color) The lowest-total-energy conformations obtained at the lowest temperature T_1 (300 K) with $\lambda=0$ (in gas phase) (a) and $\lambda=1$ (in aqueous solution) (b), and the two super imposed conformations (c). VMD software (Ref. 86) and RASTER 3D software (Ref. 87) were used to create the figures. The solid spheres are the oxygen atoms (in red) and the nitrogen atoms (in blue) in Table V.

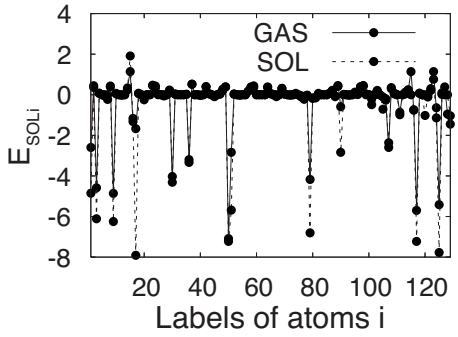

FIG. 12. The atomistic solvation free energy as a function of labels of heavy atoms for the lowest-total-energy conformations obtained at the lowest temperature T_1 (300 K) with $\lambda=0$ (in gas phase) and $\lambda=1$ (in aqueous solution).

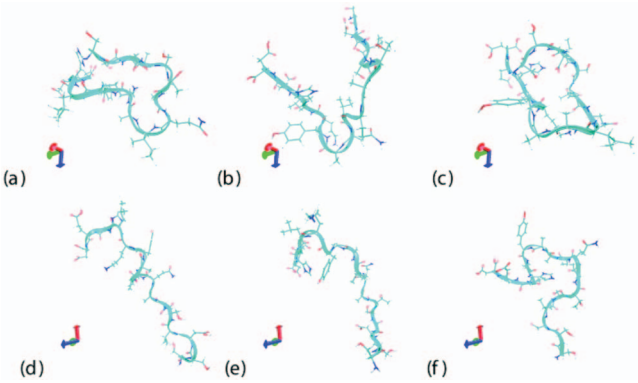

FIG. 13. (Color) Snapshots at 200 000 MC sweeps [(a) and (d)], at 600 000 MC sweeps [(b) and (e)], and at 1 000 000 MC sweeps [(c) and (f)] at the highest temperature T_8. (a)–(c) correspond to $\lambda=0$ (in gas phase) and (d)–(f) to $\lambda=1$ (in aqueous solution). VMD software (Ref. 86) and RASTER 3D software (Ref. 87) were used to create the figures.

TABLE V. Differences in the atomistic solvent-accessible surface area ΔS_i and the atomistic solvation free energy ΔE_{soli} of heavy atoms i between the lowest-total-energy conformations obtained in aqueous solution and in gas phase [i.e., $S_i(\mathrm{sol})-S_i(\mathrm{gas})$ and $E_{soli}(\mathrm{sol})-E_{soli}(\mathrm{gas})$]. We list heavy atoms of N in Ser1, OG in Ser1, OG in Ser2, OD in Asp3, NE in Gln8, OH in Tyr12, NZ in Lys13, OE in Glu16, and OD in Asp17, of which the absolute values of ΔE_{soli} are larger than 1.2 kcal/mol. The solvent-accessible surface area is in A^2 and the solvation free energy is in kcal/mol.

Residue	Ser1	Ser1	Ser2	Asp3	Gln8	Tyr12	Lys13	Glu16	Asp17
Atom	N	OG	OG	OD	NE	OH	NZ	OE	OD
Labels of atoms i	1	3	9	17	51	79	90	117	125
ΔS_i	17.03	8.88	8.08	36.34	21.51	15.34	17.03	8.88	13.73
ΔE_{soli}	−2.25	−1.53	−1.39	−6.25	−2.84	−2.64	−2.25	−1.53	−2.36

the original potential energy function E_0 by adding any physical quantities V_ℓ of interest as a new energy term with a coupling constant $\lambda^{(\ell)}(\ell=1,\ldots,L)$. The simulation in multidimensional MUCA algorithms realizes a random walk in $E_0, V_1, \ldots, V_L$ space. On the other hand, the simulations in multidimensional ST algorithms and multidimensional REM realize a random walk in temperature and $\lambda^{(\ell)}(\ell=1,\ldots,L)$ space.

While the multidimensional REM simulation can be easily performed because no weight factor determination is necessary, the required number of replicas can be quite large and computationally demanding. We thus prefer to use the multidimensional MUCA or ST, where only a single replica is simulated, instead of REM. However, it is very difficult to obtain optimal weight factors for the multidimensional MUCA and ST. Here, we have proposed a powerful method to determine these weight factors. Namely, we first perform a short multidimensional REM simulation and use the multiple-histogram reweighting techniques to determine the weight factors for multidimensional MUCA and ST simulations.

We presented the results of the two-dimensional REM simulation and the two-dimensional ST simulation. The weight factor for the ST simulation was easily obtained by the two-dimensional REM simulation and the multiple-histogram reweighing techniques. The simulations were successful in the sense that the random walk in both temperature space and λ space were realized. As far as we know, this is the first example of multidimensional ST simulations where parameters of the system (as well as temperature) are updated dynamically.

Among the three algorithms discussed in the present article, MUCA gives the most efficient sampling of configurational space resulting in the most frequent random walk, while ST gives slightly better sampling than REM.[5,62,63,65] The implementations of ST and REM are, however, simpler than MUCA because we have to change only the parameter value T or $\lambda^{(\ell)}$ during the simulation. This allows one to write a short Perl or shell script program to implement ST and REM methods without extensive modifications of the original, widely used program packages such as AMBER and CHARMM. For instance, MMTSB (Ref. 88) is a Perl program that incorporates REM into standard program packages.

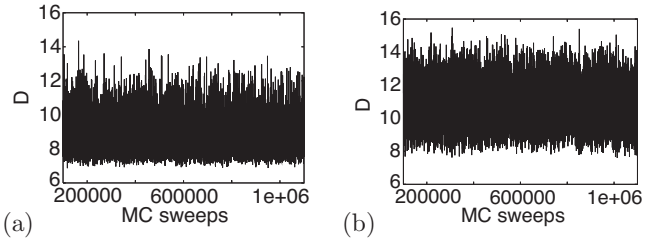

FIG. 14. Time series of the end-to-end distance with λ=0 (in gas phase) (a) and with λ=1 (in aqueous solution) (b) at the highest temperature T_8 (700 K).

There are many cases with the energy function such as systems in umbrella sampling, in magnetization with an external field, and in isobaric-isothermal ensemble, etc. The multidimensional generalized-ensemble algorithms that were presented in the present article will be very useful for MC and MD simulations of complex systems such as spin glass, molecular, polymer, and biopolymer systems.

ACKNOWLEDGMENTS

Some of the results were obtained by the computations on the super computers at the Institute for Molecular Science, Okazaki, Japan. This work was supported, in part, by Grants-in-Aid for Scientific Research in Priority Areas ("Water and Biomolecules" and "Molecular Theory for Real Systems"), for Scientific Research on Innovative Areas ("Fluctuations and Biological Functions"), and for the Next Generation Super Computing Project, Nanoscience Program from the Ministry of Education, Culture, Sports, Science and Technology (MEXT), Japan.

[1] U. H. E. Hansmann and Y. Okamoto, in *Annual Reviews of Computational Physics VI*, edited by D. Stauffer (World Scientific, Singapore, 1999), pp. 129–157.
[2] A. Mitsutake, Y. Sugita, and Y. Okamoto, Biopolymers **60**, 96 (2001).
[3] Y. Sugita and Y. Okamoto, in *Lecture Notes in Computational Science and Engineering*, edited by T. Schlick and H. H. Gan (Springer-Verlag, Berlin, 2002) pp. 304–332; e-print arXiv:cond-mat/0102296.
[4] Y. Okamoto, J. Mol. Graphics Modell. **22**, 425 (2004); e-print arXiv:cond-mat/0308360.
[5] Y. Sugita, A. Mitsutake, and Y. Okamoto, in *Lecture Notes in Physics*, edited by W. Janke (Springer-Verlag, Berlin, 2008) pp. 369–407; e-print arXiv:cond-mat/0707.3382.
[6] A. M. Ferrenberg and R. H. Swendsen, Phys. Rev. Lett. **61**, 2635 (1988); **63**, 1658 (1989).
[7] A. M. Ferrenberg and R. H. Swendsen, Phys. Rev. Lett. **63**, 1195 (1989).
[8] S. Kumar, D. Bouzida, R. H. Swendsen, P. A. Kollman, and J. M. Rosenberg, J. Comput. Chem. **13**, 1011 (1992).
[9] B. A. Berg and T. Neuhaus, Phys. Lett. B **267**, 249 (1991).
[10] B. A. Berg and T. Neuhaus, Phys. Rev. Lett. **68**, 9 (1992).
[11] A. P. Lyubartsev, A. A. Martinovski, S. V. Shevkunov, and P. N. Vorontsov-Velyaminov, J. Chem. Phys. **96**, 1776 (1992).
[12] E. Marinari and G. Parisi, Europhys. Lett. **19**, 451 (1992).
[13] K. Hukushima and K. Nemoto, J. Phys. Soc. Jpn. **65**, 1604 (1996).
[14] C. J. Geyer, in *Computing Science and Statistics: Proceedings of the 23rd Symposium on the Interface*, edited by E. M. Keramidas (Interface Foun-

dation, Fairfax Station, 1991), pp. 156–163.
[15] M. Mezei, J. Comput. Phys. **68**, 237 (1987).
[16] C. Bartels and M. Karplus, J. Phys. Chem. B **102**, 865 (1998).
[17] E. Marinari, G. Parisi, and J. J. Ruiz-Lorenzo, in *Spin Glasses and Random Fields*, edited by A. P. Young (World Scientific, Singapore, 1998), pp. 59–98.
[18] M. C. Tesi, E. J. J. van Rensburg, E. Orlandini, and S. G. Whittington, J. Stat. Phys. **82**, 155 (1996).
[19] U. H. E. Hansmann and Y. Okamoto, J. Comput. Chem. **14**, 1333 (1993).
[20] F. A. Escobedo and J. J. de Pablo, J. Chem. Phys. **103**, 2703 (1995).
[21] A. Irbäck and F. Potthast, J. Chem. Phys. **103**, 10298 (1995).
[22] U. H. E. Hansmann and Y. Okamoto, J. Comput. Chem. **18**, 920 (1997).
[23] U. H. E. Hansmann, Chem. Phys. Lett. **281**, 140 (1997).
[24] Y. Sugita and Y. Okamoto, Chem. Phys. Lett. **314**, 141 (1999).
[25] A. Irbäck and E. Sandelin, J. Chem. Phys. **110**, 12256 (1999).
[26] M. G. Wu and M. W. Deem, Mol. Phys. **97**, 559 (1999).
[27] Q. Yan and J. J. de Pablo, J. Chem. Phys. **111**, 9505 (1999).
[28] U. H. E. Hansmann, Y. Okamoto, and F. Eisenmenger, Chem. Phys. Lett. **259**, 321 (1996).
[29] N. Nakajima, H. Nakamura, and A. Kidera, J. Phys. Chem. B **101**, 817 (1997).
[30] D. Gront, A. Kolinski, and J. Skolnick, J. Chem. Phys. **113**, 5065 (2000).
[31] A. E. Garcia and K. Y. Sanbonmatsu, Proteins **42**, 345 (2001).
[32] R. H. Zhou, B. J. Berne, and R. Germain, Proc. Natl. Acad. Sci. U.S.A. **98**, 14931 (2001).
[33] G. La Penna, A. Mitsutake, M. Masuya, and Y. Okamoto, Chem. Phys. Lett. **380**, 609 (2003).
[34] M. Feig, A. D. MacKerell, and C. L. Brooks III, J. Phys. Chem. B **107**, 2831 (2003).
[35] Y. M. Rhee and V. S. Pande, Biophys. J. **84**, 775 (2003).
[36] Y. Z. Ohkubo and C. L. Brooks III, Proc. Natl. Acad. Sci. U.S.A. **100**, 13916 (2003).
[37] J. W. Pitera and W. Swope, Proc. Natl. Acad. Sci. U.S.A. **100**, 7587 (2003).
[38] H. Kokubo and Y. Okamoto, Chem. Phys. Lett. **383**, 397 (2004).
[39] A. K. Felts, Y. Harano, E. Gallicchio, and R. M. Levy, Proteins **56**, 310 (2004).
[40] A. Mitsutake, M. Kinoshita, Y. Okamoto, and F. Hirata, J. Phys. Chem. B **108**, 19002 (2004).
[41] A. E. Roitberg, A. Okur, and C. Simmerling, J. Phys. Chem. B **111**, 2415 (2007).
[42] B. A. Berg, U. H. E. Hansmann, and T. Neuhaus, Phys. Rev. B **47**, 497 (1993).
[43] W. Janke and S. Kappler, Phys. Rev. Lett. **74**, 212 (1995).
[44] S. Kumar, P. Payne, and M. Vásquez, J. Comput. Chem. **17**, 1269 (1996).
[45] C. Bartels and M. Karplus, J. Comput. Chem. **18**, 1450 (1997).
[46] Y. Iba, G. Chikenji, and M. Kikuchi, J. Phys. Soc. Jpn. **67**, 3327 (1998).
[47] B. A. Berg, H. Noguchi, and Y. Okamoto, Phys. Rev. E **68**, 036126 (2003).
[48] S. G. Itoh and Y. Okamoto, Chem. Phys. Lett. **400**, 308 (2004).
[49] J. Higo, N. Nakajima, H. Shirai, A. Kidera, and H. Nakamura, J. Comput. Chem. **18**, 2086 (1997).
[50] H. Okumura and Y. Okamoto, Chem. Phys. Lett. **383**, 391 (2004).
[51] S. G. Itoh and Y. Okamoto, Mol. Simul. **33**, 83 (2007); Phys. Rev. E **76**, 026705 (2007).
[52] Y. Sugita, A. Kitao, and Y. Okamoto, J. Chem. Phys. **113**, 6042 (2000).
[53] T. Okabe, M. Kawata, Y. Okamoto, and M. Mikami, Chem. Phys. Lett. **335**, 435 (2001).
[54] D. Paschek and A. E. Garcia, Phys. Rev. Lett. **93**, 238105 (2004).
[55] K. Murata, Y. Sugita, and Y. Okamoto, Chem. Phys. Lett. **385**, 1 (2004).
[56] C. J. Woods, J. W. Essex, and M. A. King, J. Phys. Chem. B **107**, 13703 (2003).
[57] T. W. Whitfield, L. Bu, and J. E. Straub, Physica A **305**, 157 (2002).
[58] H. Fukunishi, O. Watanabe, and S. Takada, J. Chem. Phys. **116**, 9058 (2002).
[59] S. Jang, S. Shin, and Y. Pak, Phys. Rev. Lett. **91**, 058305 (2003).
[60] W. Kwak and U. H. E. Hansmann, Phys. Rev. Lett. **95**, 138102 (2005).
[61] Y. Sugita and Y. Okamoto, Chem. Phys. Lett. **329**, 261 (2000).
[62] A. Mitsutake, Y. Sugita, and Y. Okamoto, J. Chem. Phys. **118**, 6664 (2003).
[63] A. Mitsutake, Y. Sugita, and Y. Okamoto, J. Chem. Phys. **118**, 6676 (2003).
[64] M. K. Fenwick and F. A. Escobedo, J. Chem. Phys. **119**, 11998 (2003).
[65] A. Mitsutake and Y. Okamoto, J. Chem. Phys. **121**, 2491 (2004).
[66] R. Affentranger, I. Tavernelli, and E. E. D. Iorio, J. Chem. Theory Comput. **2**, 217 (2006).
[67] G. Bussi, F. Gervasio, A. Laio, and M. Parrinello, J. Am. Chem. Soc. **128**, 13435 (2006).
[68] T. Rodinger, P. L. Howell, and R. Pomès, J. Chem. Theory Comput. **2**, 725 (2006).
[69] V. Babin, C. Roland, and C. Sagui, J. Chem. Phys. **128**, 134101 (2008).
[70] A. Mitsutake and Y. Okamoto, Phys. Rev. E **79**, 047701 (2009).
[71] A. Mitsutake and Y. Okamoto, Chem. Phys. Lett. **332**, 131 (2000).
[72] G. M. Torrie and J. P. Valleau, J. Comput. Phys. **23**, 187 (1977).
[73] H. Okumura and Y. Okamoto, Phys. Rev. E **70**, 026702 (2004).
[74] F. A. Escobedo, J. Chem. Phys. **123**, 044110 (2005).
[75] N. Metropolis, A. W. Rosenbluth, M. N. Rosenbluth, A. H. Teller, and E. Teller, J. Chem. Phys. **21**, 1087 (1953).
[76] J. K. Myers, C. N. Pace, and J. M. Scholtz, Proc. Natl. Acad. Sci. U.S.A. **94**, 2833 (1997).
[77] F. A. Momany, R. F. McGuire, A. W. Burgess, and H. A. Scheraga, J. Phys. Chem. **79**, 2361 (1975).
[78] G. Némethy, M. S. Pottle, and H. A. Scheraga, J. Phys. Chem. **87**, 1883 (1983).
[79] M. J. Sippl, G. Némethy, and H. A. Scheraga, J. Phys. Chem. **88**, 6231 (1984).
[80] T. Ooi, M. Oobatake, G. Némethy, and H. A. Scheraga, Proc. Natl. Acad. Sci. U.S.A. **84**, 3086 (1987).
[81] M. Masuya (unpublished), see http://biocomputing.cc/nsol/.
[82] H. Kawai, Y. Okamoto, M. Fukugita, T. Nakazawa, and T. Kikuchi, Chem. Lett. **1991**, 213 (1991).
[83] Y. Okamoto, M. Fukugita, T. Nakazawa, and H. Kawai, Protein Eng. **4**, 639 (1991).
[84] A. Mitsutake and Y. Okamoto, Chem. Phys. Lett. **309**, 95 (1999).
[85] A. Mitsutake and Y. Okamoto, J. Chem. Phys. **112**, 10638 (2000).
[86] W. Humphrey, A. Dalke, and K. Schulten, J. Mol. Graphics Modell. **14**, 33 (1996).
[87] E. A. Merritt and D. J. Bacon, Methods Enzymol. **277**, 505 (1997).
[88] M. Feig, J. Karanicolas, and C. L. Brooks III, J. Mol. Graphics Modell. **22**, 377 (2004); see http://mmtsb.org/.